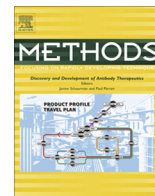




Contents lists available at ScienceDirect

Methods

journal homepage: www.elsevier.com/locate/ymeth

Single molecule fluorescence methodologies for investigating transcription factor binding kinetics to nucleosomes and DNA

Yi Luo^{a,b}, Justin A. North^a, Michael G. Poirier^{a,b,*}

^a Department of Physics, The Ohio State University, Columbus, OH 43210-1117, United States

^b Biophysics Graduate Program, The Ohio State University, Columbus, OH 43210-1117, United States

ARTICLE INFO

Article history:

Received 3 April 2014

Received in revised form 3 September 2014

Accepted 30 September 2014

Available online xxx

Keywords:

Single molecule fluorescence
Fluorescence resonance energy transfer
Transcription factors
Chromatin
Nucleosomes

ABSTRACT

Site specific DNA binding complexes must bind their DNA target sites and then reside there for a sufficient amount of time for proper regulation of DNA processing including transcription, replication and DNA repair. In eukaryotes, the occupancy of DNA binding complexes at their target sites is regulated by chromatin structure and dynamics. Methodologies that probe both the binding and dissociation kinetics of DNA binding proteins with naked and nucleosomal DNA are essential for understanding the mechanisms by which these complexes function. Here, we describe single-molecule fluorescence methodologies for quantifying the binding and dissociation kinetics of transcription factors at a target site within DNA, nucleosomes and nucleosome arrays. This approach allowed for the unexpected observation that nucleosomes impact not only binding but also dissociation kinetics of transcription factors and is well-suited for the investigation of numerous DNA processing complexes that directly interact with DNA organized into chromatin.

© 2014 Published by Elsevier Inc.

1. Introduction

The organization of DNA into chromatin fibers involves the periodic wrapping of DNA around histone protein octamers into nucleosomes [1], which is then compacted into higher order structures [2]. This compaction of DNA significantly influences the occupancy of numerous regulatory protein complexes at their DNA target sites, including transcription factors (TFs), polymerases, and DNA repair complexes [3,4]. However, the physical mechanisms by which chromatin structural dynamics regulate protein occupancy at specific DNA sites *in vivo*, remain unresolved.

A number of laboratories including ours are investigating *in vitro* the physical alterations that occur within chromatin to accommodate protein binding to DNA. Studies have quantified a variety of dynamic structural changes within chromatin, including partial DNA unwrapping, nucleosome sliding, assembly/disassembly, and transient opening of the histone octamer [2,5]. These dynamic structural changes can be induced by thermal fluctuations, chromatin remodeling and histone chaperones [2,6,7]. In this paper we focus on partial DNA unwrapping dynamics of the nucleosome that facilitates TF binding in the DNA entry/exit region, which traps the nucleosome in a partially unwrapped state. We

will discuss our recent application of single-molecule fluorescence methodologies to study such dynamics and the influence of the nucleosome on TF binding and dissociation kinetics. Ensemble fluorescence assays will also be discussed briefly as they provide essential controls for the single-molecule methods.

A fundamental property of the nucleosome is that it continually undergoes thermally induced partial DNA unwrapping, which transiently exposes DNA sites for protein binding (Fig. 1A and B). This nucleosomal DNA site exposure was first reported by Jon Widom and Kevin Polach [8] and is quantified by an equilibrium constant, K_{eq} . The K_{eq} is equal to the ratio of the DNA unwrapping rate that exposes a DNA sequence for protein binding to the DNA rewrapping rate that prevents protein binding. The site exposure equilibrium constant was initially investigated with restriction enzyme (RE) digestion measurements, which inferred K_{eq} from measured rates of RE digestion at a recognition site positioned within the nucleosome relative to the rate of cleavage of the target site within naked DNA [8]. More recently, fluorescence resonance energy transfer (FRET) measurements have been used to quantify K_{eq} by detecting partially unwrapped nucleosomes bound by a TF at its target site that is positioned within the nucleosome [9–11]. The K_{eq} for the TF binding site is determined by comparing the TF concentration required to bind 50% of its sites within nucleosomes to the TF concentration needed to bind 50% of its sites within naked DNA. Both the restriction enzyme and FRET experiments measure protein occupancy at their DNA target site and

* Corresponding author at: Department of Physics, The Ohio State University, Columbus, OH 43210-1117, United States.

E-mail address: mpoirier@mps.ohio-state.edu (M.G. Poirier).

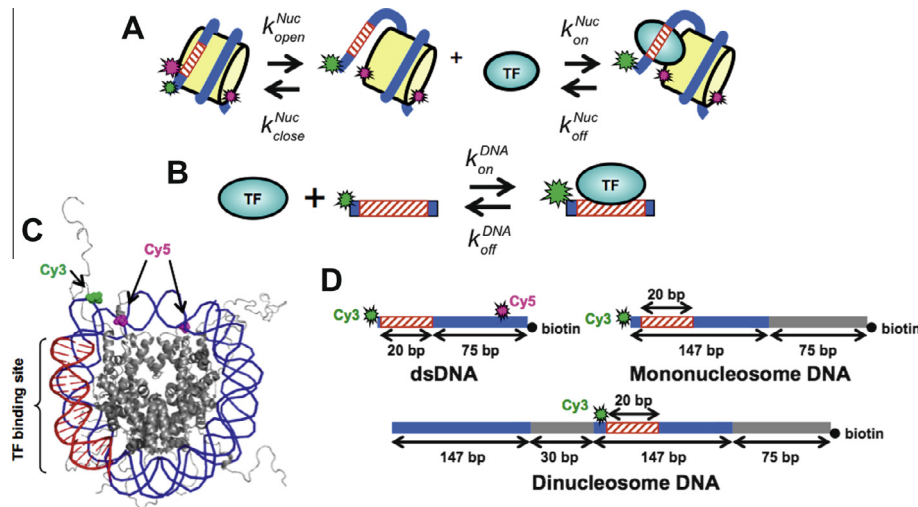


Fig. 1. Kinetic models of TF binding to (A) nucleosomes and (B) DNA. (C) Structure of the nucleosome (PDB: 1KX5), highlighting the location of the TF binding site (red), the Cy3 fluorophore (green) and the Cy5 fluorophore (magenta). (D) DNA constructs for single-molecule TIRF experiments with Cy3 (green), Cy5 (magenta), biotin (black circle), and the TF binding site (red shadow). The dsDNA used in single-molecule PIFE experiments were labeled with Cy3 and Cy5 fluorophores, while the DNA molecules that were reconstituted into mononucleosomes and dinucleosome arrays were only labeled with Cy3.

then infer K_{eq} by assuming that the binding and dissociation rates of the DNA binding protein at an exposed nucleosome site is identical to the rates at a site within naked DNA. These measurements have determined that DNA site accessibility ranges from 0.1 to 10^{-6} and exponentially decreases as a target site is positioned closer to the nucleosome dyad symmetry axis [8,12].

The use of FRET to detect nucleosome structural changes has been combined with a variety of methodologies, including stopped flow [13–15], fluorescence correlation spectroscopy (FCS) [13,14], and single-molecule fluorescence studies [16–21]. These FRET based methodologies have investigated nucleosome unwrapping, sliding and disassembly induced by thermal fluctuations, nucleosome remodeling complexes and histone chaperones. FRET based studies have revealed a number of nucleosome and chromatin properties including: DNA unwrapping is rapid (20 s^{-1}) near the nucleosome entry–exit region [13], the unwrapping rates are significantly reduced for sites further into the nucleosome [14], and histone post translational modifications (PTMs) and DNA sequence influence TF occupancy by altering the unwrapping rate [10,22–24].

Here we detail a single-molecule fluorescence methodology for directly observing single protein binding and dissociation events at its target sequence located within naked dsDNA, mono-nucleosomes and dinucleosome arrays. Our initial application of single-molecule fluorescence methodology to study TF binding dynamics in chromatin allowed for the observation that nucleosomes not only inhibit protein binding rates via steric occlusion, but also dramatically enhance protein dissociation by three orders of magnitude [25]. While our studies focused on TF binding and dissociation, these methodologies can be extended to any protein that binds a DNA target site located within the nucleosome and should be of broad utility to investigating the interactions between chromatin and the many eukaryotic site specific DNA binding proteins.

2. Experimental design

2.1. Overall strategy for detecting TF binding within nucleosomes

To directly study the dynamics of TF binding to naked DNA and nucleosomes, methods that detect both binding and dissociation are required. Stopped flow and Surface Plasmon Resonance (SPR) are ensemble techniques that can probe binding and dissociation

kinetics. Both techniques rapidly shift the ligand (TF) concentration and then detect the time evolution of the ligand–receptor (DNA or nucleosome) binding as the system relaxes to a new binding equilibrium. However, there are challenges to each of these methodologies for investigating TF binding to and dissociation from naked DNA and/or nucleosomes. While stopped flow has previously been used to detect the rate of TF binding to both naked DNA [26–28] and nucleosomes [13–15,24], detection of TF dissociation by stopped flow is problematic. Measuring the rate of dissociation by rapidly diluting DNA–TF complexes would require dramatic dilutions of DNA that makes detection challenging. Moreover, rapidly diluting nucleosomes can result in spontaneous nucleosome disassembly among other issues [29]. Alternatively, rapidly mixing excess DNA that contain the TF target site can be used to quickly deplete the concentration of unbound TF. However, addition of competitor DNA can bind with partially bound TF states and result in observed dissociation rates that are much higher than the inherent rate of TF dissociation [30–33].

Surface Plasmon Resonance has been used to measure the binding and dissociation rates of TFs with naked DNA [34–36]. However, this approach is challenging with nucleosomes because following each injection of the TF a high salt wash is required to remove the remaining TF. This will cause nucleosomes to disassemble following each wash, making SPR impractical for measuring TF binding with nucleosomes. Finally, these techniques observe kinetics by rapidly shifting the system out of equilibrium and then observing the time to relax back. This non-equilibrium approach assumes that the system responds linearly to the perturbation, which is not necessarily the case.

An alternative approach to studying ligand–receptor binding and dissociation is single molecule fluorescence measurements [37]. We constructed a single molecule fluorescence system, and prepared fluorophore labeled DNA and nucleosomes for detection of TF binding and dissociation (Fig. 1C and D). This approach has the advantage of detecting TF–DNA and TF–nucleosome binding and dissociation while each ligand–receptor system is in equilibrium.

2.2. Design for detecting TF binding within partially unwrapped nucleosomes

We aim to track the binding of a TF to its target site within a nucleosome. As the nucleosome undergoes spontaneous

unwrapping, the distance between the unwrapped DNA and the histone octamer core increases (Fig. 1A). This change in distance can be tracked by FRET if the donor and acceptor fluorophores are placed separately on DNA and histone octamer. The donor and acceptor are within a few nanometers of each other in the fully wrapped nucleosome, which results in high FRET efficiency since it is less than the Cy3/Cy5 Förster radius (R_0) of ~ 6 nm. As the DNA unwraps the distance between the donor and acceptor increases, resulting in a significant reduction in FRET efficiency. The spontaneous unwrapping to expose a TF site within the nucleosome entry–exit region occurs at a rate of about 20 s^{-1} , while the rewinding occurs with a rate that is over an order of magnitude faster [13]. Therefore, the rapid unwrapping and rewinding cannot be directly detected by an EMCCD camera that is used for single molecule fluorescence measurements, which have a maximum acquisition frame rate of 20 Hz [25]. At this acquisition rate, the nucleosomes are measured to have a constant FRET efficiency of about 80% [25]. However, the binding of a TF to a partially unwrapped nucleosome traps it in the open conformation for a time long enough that the reduction in FRET efficiency can be detected by an EMCCD camera. Once the TF dissociates the partially unwrapped nucleosome then rapidly rewraps. Thus, tracking changes in the DNA–histone distance near the nucleosome entry–exit region via changes in FRET efficiency provides detection of TF binding to and dissociating from a partially unwrapped nucleosome.

We chose to study the TF binding to its recognition site near the entry–exit region of a nucleosome since many TF binding sites are located near this region of a nucleosome *in vivo* [38–41], indicating that the unwrapping dynamics can be important for the regulation of gene expression. We separately inserted the LexA and Gal4 binding sites between the 8th and the 27th, and the 8th and the 26th base pairs of the nucleosomal DNA (Fig. 1D), respectively, which oriented the TF binding surface toward the histone octamer. We attached the Cy3 and Cy5 fluorophore pair to the DNA and histone octamer, respectively, near the entry–exit region to detect nucleosome unwrapping (Fig. 1C). We chose these fluorophores because (i) they have good quantum yield and photo-stability at physiologically relevant conditions, (ii) the Cy3–Cy5 Förster radius of 6 nm provides a good dynamics range for detecting nucleosome unwrapping and (iii) Cy3–Cy5 has been used extensively in FRET studies of nucleosomes [9,11,18,19,22,24].

As with previous ensemble measurements, we attached the donor Cy3 fluorophore to the DNA because this can be done with essentially 100% efficiency allowing us to determine the FRET efficiency by the (ratio)_A method [42]. The acceptor Cy5 fluorophore was attached to the histone octamer near the DNA entry–exit region at H2A(K119C) (Fig. 1C). Since the H2A–H2B heterodimer is first to dissociate from a fully formed nucleosome [43], we used the direct excitation of Cy5 fluorescence to ensure that each molecule we studied was a fully formed nucleosome [25]. There is one native cysteine in the histone octamer at H3(C110), which was mutated to an alanine. This mutation has been used in combination with site-specific fluorophore labeling in the histone octamer and has minimal impact on nucleosome structure and dynamics [23,44].

In vivo nucleosomes are embedded into long chromatin molecules, which consists of repeating chains of regularly spaced nucleosomes. Therefore, it is essential to measure DNA–protein interactions within the context of nucleosome arrays. Short nucleosome arrays can be constructed *in vitro* to mimic the chromatin fiber and study the influence of adjacent nucleosomes and linker DNA on nucleosome structure and dynamics [45–48]. We designed a dinucleosome array with FRET labels to study the TF binding within a nucleosome that is adjacent to a second nucleosome. This array is comprised of two nucleosomes, one with a TF binding site and the other without, connected by a 30 bp linker DNA. The TF binding site is placed at the entry/exit region of one nucleosome

close to the linker DNA. The donor Cy3 fluorophore is attached to the 4th nucleotide of the 147 bp 601 nucleosome positioning sequence containing the TF binding site (Fig. 1D), while the acceptor Cy5 fluorophore is again attached to H2A(K119C).

The single molecule fluorescence measurements require that the mono- and dinucleosomes are tethered to a quartz microscope slide by a biotin–streptavidin–biotin linkage [49]. We chose to attach biotin to the 5-prime end of a 75 bp extension arm on the side of the 147 bp 601 nucleosome positioning DNA sequence opposite to the TF recognition site (Fig. 1D). This additional DNA extends the mono- and dinucleosomes away from the surface to reduce non-specific interactions that could influence nucleosome stability and the unwrapping dynamics. Also, by placing the TF binding site opposite to the surface attachment, the influence of the surface attachment on nucleosome unwrapping dynamics and TF binding is minimized.

2.3. Design of naked DNA molecules for detecting TF binding and dissociation

To understand how nucleosome dynamics influences TF binding, we need to compare kinetics of TF binding to and dissociating from a nucleosomal DNA site to a site within naked DNA. While surface plasmon resonance or stopped-flow fluorescence detection can be used to characterize the protein–DNA interaction kinetics, we chose to use single molecule fluorescence, which has distinct advantages as discussed above. One option is to label the TF protein and DNA separately and track the co-localization of the two color signals to determine binding and dissociation. However, this approach is limited by a few factors, including protein labeling efficiency, fluorophore photobleaching, non-specific interaction of the labeled protein and the increase in fluorescence background for protein concentrations above 10 nM [37]. Instead, we used Protein-Induced Fluorescence Enhancement (PIFE) [50], where a change in fluorescence quantum yield of a fluorophore is induced upon protein binding at the site nearby (Fig. 1B). PIFE detection does not require labeling of protein, and thus it is not limited by the protein labeling efficiency or concentration. The level of fluorescence emission is sensitive to the distance between the fluorophore and the protein–DNA interaction site. We used a Cy3 fluorophore attached near the TF specific target sequence so that the detection is only sensitive to the specific interaction at the target site. We confirmed that PIFE detects TF binding to its target site and does not alter the TF dissociation constant by comparing these measurements to Electrophoretic Mobility Shift Assays (EMSA) [25].

The designs of the DNA molecules for single-molecule PIFE studies are similar to the designs of DNA molecules used in the nucleosome measurements. We included 75 bp of DNA on one end of the specific TF-binding sequence (Fig. 1D) to extend the target site away of the quartz surface. A biotin was attached to the 5'-end of the extension arm for tethering the molecule to the streptavidin treated quartz surface. The Cy3 fluorophore was positioned on the other end of the DNA, 1 bp away from the TF-binding sequence. While a single Cy3 fluorophore alone is sufficient for detection of PIFE signal upon TF binding, we attached a second fluorophore, Cy5, to increase the certainty that the location of Cy3 fluorescence is a DNA molecule. Only DNA molecules that had both Cy3 and Cy5 signals were selected for PIFE analysis. We attached the Cy5 fluorophore at an internal site close to the biotin end, 70 bp from the TF binding site, so it would not interfere with PIFE or TF binding and dissociation.

2.4. Preparation of DNA molecules

The consensus target sequence for LexA (5'-TACTGTATGAGC ATACAGTA) was inserted to the 601 nucleosome position sequence

at base pairs 8–27, and the consensus sequence for Gal4 (5'-CCGG AGGACTGTCTCCGG) was inserted at base pairs 8–26. These target sequences were inserted into the 601 sequence using PCR with primers that contain the TF target sequence, which was then cloned into the pDrive (Qiagen) vector.

The dsDNA molecules for reconstituting mono-nucleosomes and for the PIFE experiments were synthesized by PCR using Cy3, Cy5 or biotin labeled oligonucleotides as primers (Table 1) and a plasmid containing the modified 601 sequence with the TF target site as the template. Oligonucleotides with an amine group modification at the 5'-end or on an internal modified thymine base (Sigma) were labeled with Cy3- or Cy5-NHS ester (GE Healthcare). Oligonucleotide labeling was performed using a 5–10-fold molar excess of Dye in 0.1 M Na₂B₄O₇ pH 8.5 at room temperature for 12 h. After the labeling reaction, the oligonucleotides were purified by reverse-phase HPLC on a 218TP C18 column (Grace/Vydac), and then used in as primers for PCR. Each dsDNA molecule synthesized by PCR was purified by HPLC on a Gen-Pak Fax ion-exchange column (Waters).

The DNA molecules used for reconstituting dinucleosome arrays were prepared by ligating two shorter PCR-synthesized DNA segments. In our design of the DNA for the dinucleosome array, a nonpalindromic TspRI restriction site was inserted into the linker DNA between the two 601 nucleosome positioning sequences. Each of the two shorter segments contains one 601 sequence and part of the linker DNA including the TspRI site. Segment 1 contains the original 601 sequence with no fluorophore label (Fig. 1D), and it was synthesized using unlabeled primers (Table 1). Segment 2 contains the 601 sequence with the LexA binding site, the donor fluorophore Cy3 attached to a dT and the 75 bp extension with a 5' end biotin (Fig. 1D). It was synthesized using Cy3 and biotin labeled primers (Table 1). These two DNA segments were purified by phenol extraction following PCR and then digested by TspRI in NEB buffer 4 (New England Biolabs), which results in a 9 base pair 3' single strand overhang. The TspRI digested segments were purified by polyacrylamide gel electrophoresis (PAGE) to remove the short TspRI fragments. The purified segments with 9 bp single strand overhangs were then combined at equal molar ratio and ligated by T4 ligase (New England Biolabs) in the supplied buffer with additional 2 mM ATP. The ligated DNA molecule with two 601 sequences was purified by HPCL using a Gen-Pak Fax column (Waters).

2.5. Preparation of acceptor-labeled histone octamer

Recombinant *Xenopus laevis* histones were used for reconstituting nucleosomes. All core histones: H2A(K119C), H2B, H3(C110A) and H4 were expressed individually in *Escherichia coli* BL21(DE3)-pLysS cells (Invitrogen) and purified as previously described [51].

The four purified core histones were then combined at equal molar ratios, refolded into octamers and labeled with Cy5-maleimide (Amersham) as previously described [23]. Labeled histone octamers were then purified by size-exclusion FPLC on a Superdex 200 GL column (GE Healthcare) equilibrated with 2 M NaCl, 10 mM Tris, pH 8.0, 1 mM EDTA. The labeling efficiency of the purified octamer was assessed by absorption spectroscopy and was normally around 0.8–0.9 (Cy5/H2A molar ratio).

2.6. Nucleosome reconstitution

Nucleosomes were reconstituted by double dialysis using purified Cy3–biotin-labeled DNA and Cy5 labeled histone octamer (HO) as previously described [23]. Briefly, for mono-nucleosomes, DNA and HO were mixed at a molar ratio of 1:0.85 (DNA:HO). For dinucleosome array, DNA and HO were mixed at a molar ratio of 0.53:1 (DNA:HO). DNA and HO were mixed in 0.5× TE buffer with 1 mM benzamidine hydrochloride (BZA) and 2 M NaCl in a volume of 50 μl. The reconstitution mix was loaded into a small dialysis chamber made from 0.8 ml PCR tubes, which was then placed into a large dialysis tube containing 80 mL of 0.5× TE, 1 mM BZA and 2 M NaCl. The large dialysis tube was dialyzed against 4 L of 0.5× TE and 1 mM BZA with at least one buffer change. Dialyzed nucleosomes were purified by sucrose gradient in an Optima L-90K Ultracentrifuge (Beckman Coulter) with a SW41 rotor. The mono-nucleosomes were purified on a 5–30% w/v sucrose gradient, and dinucleosome arrays were purified on a 5–35% w/v sucrose gradient. The purified nucleosomes were assessed by PAGE and determined to be over 95% pure.

2.7. Preparation of transcription factors

Transcription factors LexA and Gal4 were used as model factors. LexA protein was expressed recombinantly from pJWL288 plasmid and purified as previously described [52]. Gal4 expression plasmid was constructed by cloning the Gal4 gene encoding for amino acid residues 1–147 from *Saccharomyces cerevisiae* genomic DNA into pET3a plasmid. Gal4 protein was expressed and purified as previously described [25].

3. Experiment setup

3.1. Ensemble fluorescence experiments

Site accessibility for TF binding to partially unwrapped nucleosomes can be assessed from a FRET titration curve [25] by determining the S_{0.5} value, which is the concentration of TF required to bind 50% of the nucleosomes. The TF binding to its target site

Table 1
List of DNA oligos used for preparing the fluorophore labeled DNA molecules.

DNA	Primer	Sequence
dsDNA-LexA	Forward	AminoC6-5'-ATACTGTATGAGCATACAGTACAATTGGTCGTAGCAAGCT-3'
	Reverse	Biotin-5'-CCCCTTGGCGTTAAAACG[aminoC6dT]GGGGGACAGC-3'
dsDNA-Gal4	Forward	5'-CTGGAG[aminoC6dT]CCGGAGGACTGTCTCCGGTCAATTGGTCGTAGACAGCTCTAGCACCGC-3'
	Reverse	Biotin-5'-CCCCTTGGCGTTAAAACG[aminoC6dT]GGGGGACAGC-3'
nucDNA-LexA	Forward	AminoC6-5'-CTGGAGATACTGTATGAGCATACAGTACAATTGGTC-3'
	Reverse	Biotin-5'-CGCATGCTGCAGACGCGTT-3'
nucDNA-Gal4	Forward	AminoC6-5'-CTGGAGACCGGAGGGCTGCCCTCCGGTCAATTGGTC-3'
	Reverse	Biotin-5'-CGCATGCTGCAGACGCGTT-3'
dinucDNA-601	Forward	5'-CTGGAGAATCCCGTGCCG-3'
	Reverse	5'-CTAGCGTCAACCCAGTGTACAGGATGTATATATCTGACACGTGCCTGG-3'
dinucDNA-601L	Forward	5'-AGCTTGTGCAGCAATTGATCATAAGGAGGACACTGGGACATGCATCGGCTG[aminoC6dT]AGATACTGTAT-3'
	Reverse	Biotin-5'-CGCATGCTGCAGACGCGTT-3'

traps the nucleosome in the open conformation and results in reduced FRET efficiency. To measure the FRET efficiency, the fluorescence emission spectra of the FRET labeled nucleosomes were acquired using a Fluoromax 4 fluorometer (Horiba). During the titration, the concentration of FRET labeled nucleosomes was fixed, while the concentration of the TF was varied. The TF binding titrations were done at nucleosomes concentrations that were significantly below the $S_{0.5}$. This ensures that the $S_{0.5}$ depends on the site accessibility and not simply on the stoichiometry of the TF and nucleosomes. LexA titrations were done with 5 nM nucleosomes in buffer containing 50 mM HEPES, pH 7.5, 130 mM NaCl, 10% Glycerol, 0.005% TWEEN20, 0.1 mg/ml bovine serum albumin (BSA), 2 mM Trolox (Sigma 238813), 0.0115% v/v Cyclooctatetraene (COT, Sigma 138924), and 0.012% v/v 3-Nitrobenzyl alcohol (NBA, Sigma 146056) in a volume of 60 μ l. The Trolox, COT and NBA are triple state quenchers that are required in the single molecule measurements to reduce the rate of photobleaching. However, we found that these did not alter the $S_{0.5}$ ensemble measurements so they do not need to be included in the ensemble titrations. Gal4 titrations were done with 0.2 nM nucleosomes in 10 mM Tris-HCl, pH 8.0, 130 mM NaCl, 10% Glycerol, and 0.005% TWEEN20 in a volume of 2 mL. The BSA was not included so to reduce background fluorescence, which was required because the Gal4 titrations were done with a low nucleosome concentration of 0.2 nM. The donor spectra were acquired from 530 nm to 750 nm with excitation at 510 nm, while the acceptor spectra were acquired from 630 nm to 750 nm with excitation at 610 nm (Fig. 2A and B). The FRET efficiency was then calculated using the $(\text{ratio})_A$ method [42] based on the donor and acceptor spectra as previously described [23]. The FRET efficiency as a function of TF concentration was then fit to a non-cooperative ligand–receptor binding curve using Origin software (OriginLab) to determine the $S_{0.5}$ value (Fig. 2C). This $S_{0.5}$ can be interpreted as the effective dissociation constant of the TF binding to the nucleosome.

TF binding to naked DNA was determined with PIFE during a TF titration. Fluorescence emission spectra of Cy3 from 530 nm to 750 nm were acquired using an excitation of 510 nm. LexA titrations were done with 0.2 nM fluorophore labeled DNA in 10 mM Tris-HCl, pH 8.0, 130 mM NaCl, 10% Glycerol, 0.005% TWEEN20, 0.1 mg/ml BSA, and 1% β -mercaptoethanol (BME). Gal4 titrations were done with 0.1 nM fluorophore labeled DNA in 10 mM Tris-HCl, pH 8.0, 130 mM NaCl, 10% Glycerol, 0.005% TWEEN20, and 1% BME. The Cy3 PIFE emission during the titration was fit to a non-cooperative ligand–receptor binding curve using Origin software. Control TF titrations were performed with dsDNA that did not have the specific target sequence. No Cy3 fluorescence enhancement was observed using these DNA molecules [25], indicating that the PIFE measurement is sensitive only to the TF binding to its recognition site.

3.2. Single-molecule total-internal reflection fluorescence microscope

Single-molecule total-internal reflection fluorescence (smTIRF) microscopy takes advantage of the evanescent wave created by the total-internal reflection of the excitation light to illuminate only the sample molecules immobilized on the microscope slide surface, largely eliminating background fluorescence. When the concentration of the tethered molecules is low enough, we can resolve the fluorescence emission from single molecules in the microscope image of the surface. The use of a high sensitivity EMCCD camera allows tracking of the time-dependent fluorescence intensity changes in these molecules to study the molecular dynamics that cause such changes.

A prism based smTIRF microscope was built on an IX71 inverted microscope body (Olympus) [49] (Fig. 3A). 532 nm and 638 nm diode lasers (CrystalLaser) were used to excite the donor and acceptor fluorophores, respectively. The lasers were placed on custom built bases and bandpass fluorescence filters Brightline 531/22 and 640/14 (Semrock) were used to filter out wavelengths other than the 532 nm and 638 nm excitation beams, respectively. The two excitation beams were then merged into the same optical path with a Brightline 580 nm dichroic filter (Semrock) placed at 45°. The excitation beam was focused using a converging lens with 250 mm focal length and guided to the microscope objective by a mirror on a 6-axis mount. A right-angle quartz prism (Melles Griot) was used to guide the excitation beam to the flow cell surface at an angle larger than the critical angle for total internal reflection. A custom made prism holder was used to fix the position of the prism relative to the excitation beam path while still allowing free horizontal movement of the flow cell.

The single-molecule fluorescence emission was collected by a 60 \times water immersion objective (UPlanSApo 60 \times /1.20w, Olympus). Images of the Cy3 and Cy5 fluorescence were then split into separate images using a DualView system (Optical Insights) with a dichroic mirror (Chroma Technology, T6351pxr), and two bandpass filters with 30 nm bandwidth centered at 585 nm (Chroma Tech., D585/30) and at 680 nm (Chroma Tech., D680/35) for the Cy3 and Cy5 channels, respectively (Fig. 3A). The images from the two fluorophores were aligned side by side so that each of them occupies one half of the surface area on the CCD chip in a PhotonMax EMCCD camera (Princeton Instruments).

3.3. Microscope flow cell preparation

The flow cells used in the smTIRF microscope were assembled using quartz microscope slides (G. Finkenbeiner) and glass coverslips (Fig. 3B). Inlet and outlet holes were drilled into the quartz slides. A layer of Parafilm (American National Can) with cut flow channels was placed between the quartz slide and coverslip and

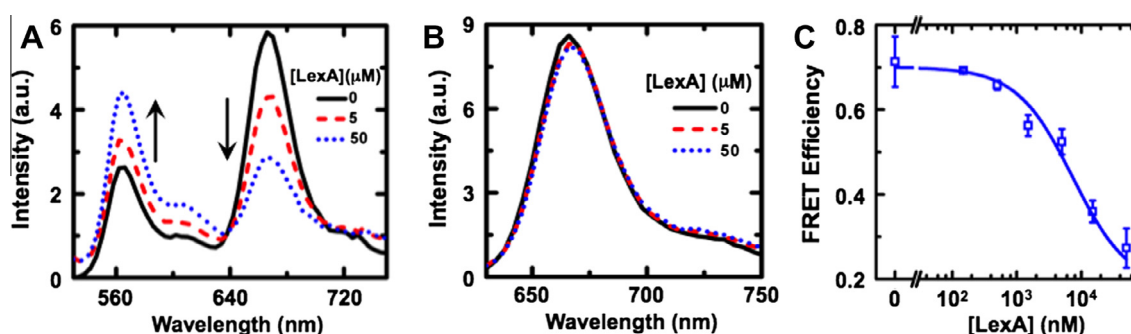


Fig. 2. (A) Fluorescence emission spectra at 0 μ M (black solid), 5 μ M (red dash), and 50 μ M (blue dot) LexA, with nucleosomes containing the LexA target site while exciting the Cy3 donor fluorophore at 510 nm. (B) Fluorescence emission spectra at 0 μ M (black solid), 5 μ M (red dash), and 50 μ M (blue dot) LexA, with nucleosomes containing the LexA target site while exciting the Cy5 acceptor fluorophore at 625 nm. (C) Ensemble mononucleosome FRET efficiency measurements of LexA titrations. The FRET efficiency (blue square) was calculated using $(\text{ratio})_A$ method and fit to a binding curve with a Hill coefficient equal to 1 (blue line).

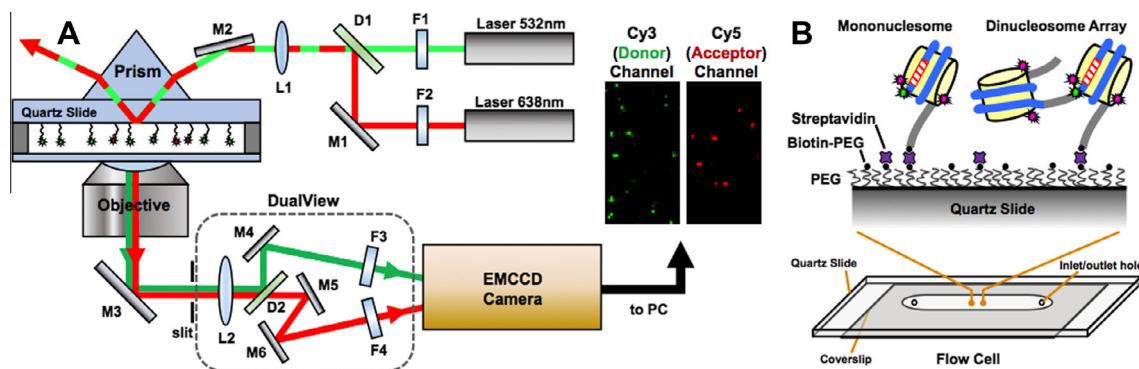


Fig. 3. (A) Schematic diagram of the prism-based single-molecule TIRF microscope setup. The optics components include mirrors (M1–6), band-pass filters (F1–4), dichroic mirrors (D1–2) and converging lenses (L1–2). The excitation laser beam was focused on the flow cell through the prism. M2 was positioned with a six-axis mount to adjust the incident angle of the laser beam. The fluorophore labeled sample molecules were illuminated by the evanescent wave created by the total internal reflection at the quartz–water interface. The fluorescence emission was collected by the objective and split into the donor and acceptor channels by the DualView and then imaged on CCD chip side by side. (B) Microscope flow cell design and slide surface functionalization. The flow cell was made by attaching the glass coverslips to the quartz slide using parafilm with cut flow channels. The quartz slide surface is functionalized with PEG and biotin-PEG. Biotinylated sample molecules were tethered on the slide surface through the biotin–streptavidin–biotin interaction. The mononucleosome and a dinucleosome array are made using the DNA constructs as shown in Fig. 1D.

heated to 100 °C to seal the cell. During the single-molecule experiment, the prism is placed on the quartz slide side of the flow cell with immersion oil to match the quartz index of refraction.

Before assembly, the quartz slides and glass coverslips were cleaned by sonication in toluene and then ethanol for 20 min each, and then by Piranha solution (3:1 mixture of concentrated sulfuric acid to 50% hydrogen peroxide). The cleaned slides and coverslips were washed in 1 M NaOH and then treated with 2% v/v 3-aminopropyl-triethoxysilane (MP Biomedicals) in anhydrous acetone. The silanized surface was then functionalized with monofunctional-PEG (Laysan Bio, MPEG-SVA-5000) and biotin-PEG (Laysan Bio, Biotin-PEG-SVA-5000) so that the fluorophore-labeled molecules can be passively immobilized on the slide surface through biotin–streptavidin–biotin linkage. 10% w/v PEG solution in 0.1 M potassium tetraborate, pH 8.1 containing a mixture of biotin-PEG and MPEG at a mass ratio of 1:100, respectively, was applied to the silanized surface and then incubated at room temperature for 1 h. After the incubation, excess amount of PEG was washed off using deionized water. The quartz slides and coverslips were air dried and then assembled into flow cells as described above.

Immediately before each single-molecule experiment, a channel within a flow cell was incubated with 1 mg/ml BSA in wash buffer (10 mM Tris–HCl, pH 8.0, 130 mM NaCl, 10% Glycerol and 0.005% TWEEN20) for 5 min. This was followed by incubating with 20 µg/ml streptavidin in wash buffer for 5 min. Excess streptavidin was then removed by flowing excess wash buffer through the flow cell. Biotinylated nucleosome or DNA samples were then flowed into the channel and incubated for 5 min to form single-molecule tethers. Before observation on the microscope, the appropriate imaging buffer was flowed into the flow channel. The imaging buffer for FRET experiments contains: 50 mM HEPES, pH 7.5, 130 mM NaCl, 10% v/v glycerol, 0.005% v/v TWEEN20, 0.1 mg/ml BSA, 2 mM Trolox, 0.0115% v/v COT, 0.012% v/v NBA. Reagents including Trolox, COT and NBA were used as triplet state quencher to improve the photo-stability of Cy3 and Cy5 fluorophores [53]. The imaging buffer for PIFE experiments contains: 10 mM Tris–HCl, pH 8.0, 130 mM NaCl, 10% v/v glycerol, 0.005% v/v TWEEN20, 0.1 mg/ml BSA, 1% v/v BME. Here BME was used as the triplet state quencher instead of Trolox, COT and NBA, because under our experimental condition BME has better effect in stabilizing Cy3 emission for long time observation, which is essential for tracking slow TF binding and dissociation events using PIFE. In addition, it has been shown that BME can promote a long-lived dark state of Cy5 [54]. Such instability in Cy5 emission prevents the use of BME in the FRET

experiments, whereas in the PIFE experiments it does not have a high impact because only Cy3 emission was tracked and Cy5 was only excited for a very short time to determine molecule location. An oxygen scavenging system containing 1.6% w/v glucose, 450 µg/ml glucose oxidase (Sigma G2133) and 22 µg/ml catalase (Sigma C3155) was also included with the imaging buffer for FRET and PIFE experiments to suppress photobleaching of the fluorophores [49]. Finally, the TF at the desired concentration was included in the imaging buffer before flowing it into the flow cell.

3.4. Data acquisition

The flow cell was mounted onto the microscope stage after the addition of imaging buffer with the TF. For the single-molecule FRET experiments, the fluorescence emission images in both Cy3 and Cy5 channels were acquired by the EMCCD camera while the donor Cy3 was excited with the 532 nm laser. The image time series was recorded onto a PC using WinView (Roper Scientific). As a nucleosome could lose part or all of its histone octamer during interaction with the microscope slide surface, we need to confirm the integrity of each nucleosome by verifying the co-localization of Cy5 fluorophore on H2A and the Cy3 fluorophore on DNA. At the beginning of each fluorescence time series, the acceptor excitation laser (638 nm) was turned on for 10 frames to locate molecules with Cy5 emission, then switched to the donor excitation laser (532 nm). During the donor excitation, the molecules that were located by direct acceptor excitation could be grouped into one of the following categories: (1) emission in Cy3 channel (low FRET), (2) emission in Cy5 channel (high FRET) or (3) no emission in either Cy3 or Cy5 channel (donor lost or photobleached). Molecules that belong to category (1) and (2) contain both Cy3 and Cy5 and thus are very likely to be complete nucleosomes. In our study only these molecules were selected for further analysis. A similar strategy was used in the single-molecule PIFE experiments. The molecules were first excited with the 638 nm laser for 10 frames to detect Cy5 fluorescence from the DNA. Then the laser excitation was switched to 532 nm to detect Cy3 fluorescence fluctuations caused by TF binding and dissociation.

In single-molecule fluorescence experiments, good signal-to-noise ratio (SNR) is critical for high quality data, but the fluorescence emission from a single fluorophore is limited. Two ways to improve SNR are to adjust the camera settings and excitation laser output. The working temperature of the EMCCD camera should be set to the lowest possible value (–80 °C for us) to suppress thermal

noise. Pixel binning can be used to obtain higher SNR at the cost of losing spatial resolution. We used 2×2 binning on a 512×512 pixel EMCCD chip. The excitation laser output power and the frame acquisition rate should be adjusted to improve SNR. Higher excitation laser power enhances fluorescence emission and thus improves the SNR, but at the cost of faster photobleaching, which reduces the acquisition time. A slower acquisition frame rate will collect more photons in each frame, improving the SNR, while preserving the acquisition time. However, this reduces the time resolution.

We applied the following rules when adjusting the acquisition rate and laser power in order to optimize the single-molecule fluorescence time series for both resolution and duration: (i) the frame rate should be significantly faster than the rate of the fluorescence fluctuation caused by the molecular interaction studied to accurately quantify each dwell time, (ii) the excitation laser output power should be adjusted so that fluorophores photobleach at a significantly slower rate than the fluorescence fluctuation rates so that multiple fluctuations are detected in each time series, and (iii) the length of the time series should be long enough so that most of the fluorophores photobleached before the end of the

acquisition so the number of molecules at each fluorescent spot can be verified by the photobleaching steps.

To determine the optimal data acquisition parameters, we carried out some preliminary measurements at about 5 Hz. For the nucleosome measurements with LexA, the TF binding/dissociation rates were relatively fast, so we used our fastest acquisition rate of 20 Hz to capture the FRET fluctuations with relatively high 532 nm laser output power of 20 mW to increase fluorescent signal. For the nucleosome experiments with Gal4 the FRET fluctuation were slower than with LexA. We acquired images at 5 frames per second with a 532 nm laser power of 20 mW. For the DNA measurements with LexA and Gal4, the PIFE fluctuation were even slower. So we acquired images at 1 frame per second with a lower 532 nm laser power of 5 mW to reduce the Cy3 photobleaching rate. The 638 nm laser power was always set to 15 mW since we only excite with 638 nm for about 1 s to determine which molecules have both Cy3 and Cy5 fluorescence emission.

Due to the limited length of time one can observe the fluorescence emission from a single fluorophore, and the possible perturbation of the interaction dynamics caused by surface tethering, fluorescence fluctuations from many single molecules must be

Table 2

List of time and rate constants measured from single-molecule experiments.

	τ_{bound} (s)	$\tau_{unbound}$ (s nM)	k_{off} (s^{-1})	k_{on} (s^{-1} nM $^{-1}$)	K_D (nM) ^a	$S_{0.5}$ (SM) (nM) ^b	$S_{0.5}$ (ENS) (nM) ^c
LexA-DNA	290 ± 20	20 ± 6	$(3.4 \pm 0.2) \times 10^{-3}$	0.05 ± 0.01	0.07 ± 0.02	0.08 ± 0.01	0.034 ± 0.004
LexA-monoNuc	0.31 ± 0.05	$(1.1 \pm 0.3) \times 10^{-4}$	3.3 ± 0.6	$(9 \pm 2) \times 10^{-5}$	$(4 \pm 2) \times 10^4$	$(3.1 \pm 0.6) \times 10^4$	7000 ± 1000
LexA-diNuc	0.29 ± 0.05	$(1.1 \pm 0.3) \times 10^{-4}$	3.5 ± 0.3	$(9 \pm 2) \times 10^{-5}$	$(4 \pm 1) \times 10^4$	$(3.7 \pm 0.3) \times 10^4$	8000 ± 1000
Gal4-DNA	$\gg 2000$	ND	$\ll 5 \times 10^{-4}$	ND	ND	ND	0.042 ± 0.006
Gal4-monoNuc	50 ± 2	2.5 ± 0.1	0.020 ± 0.001	0.40 ± 0.02	0.051 ± 0.005	0.035 ± 0.003	0.119 ± 0.004

^a K_D calculated from the ratio of single-molecule on/off rates, $K_D = k_{off}/k_{on}$.

^b $S_{0.5}$ from fitting average TF occupancy data obtained in single-molecule PIFE or FRET experiments.

^c $S_{0.5}$ from fitting ensemble PIFE or FRET titration curve.

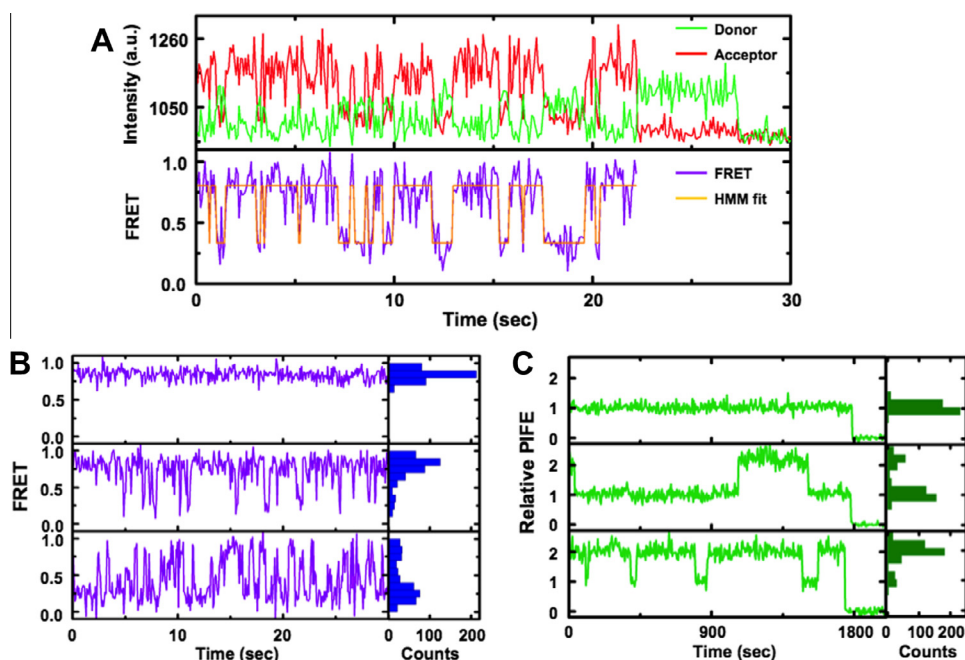


Fig. 4. (A) An example FRET time series from a single mononucleosome showing fluctuations upon LexA binding and dissociation. The raw Cy3 (green) and Cy5 (red) intensity traces were shown in the upper panel. The traces exhibit the acceptor photobleaching followed by the donor photobleaching. The FRET trace (purple) was calculated based on the raw intensity of the donor and acceptor with background subtraction and detection correction up to the acceptor photobleaching event. The measured FRET trace was fit using a hidden Markov method (HMM) resulting in an idealized FRET trace (orange). (B) Example single-molecule FRET traces of mononucleosome with LexA concentrations of 0 (top), 5 (middle), and 50 (bottom) μ M. The histogram on the right shows the FRET distribution. (C) Example single-molecule PIFE traces of LexA binding to Cy3 labeled dsDNA with LexA concentration of 0 (top), 0.1 (middle), and 1 (bottom) nM. Each trace shows the Cy3 photobleaching close to the end of the time series. The histogram on the right shows the Cy3 intensity distribution.

acquired to build up statistics for an accurate determination of the binding and dissociation kinetics. For the nucleosome experiments with LexA and Gal4 and the DNA experiments with LexA, we acquired data from over 200 molecules, which provided over 1000 single molecule TF binding and dissociation events at each concentration. For each type of experiments, the single-molecule titration was repeated for minimum of 3 times at each concentration using different flow cells to average the possible difference from flow cell and imaging buffer preparations. For the DNA experiments with Gal4, the binding and dissociation rates are so slow that many of the time traces did not show fluctuations. We acquired PIFE data on over 200 molecules but only observed single dissociation events in 7% of the time traces. Therefore, we were only able to put a limit on the dissociation rate and were not able to measure the binding rate (Table 2).

To confirm that our measurements of LexA binding to and dissociating from DNA captured most of the binding and dissociation events, we compared the fraction of DNA molecules bound by LexA measured by ensemble and single molecule measurements. We found that these independent measurements agree, which demonstrates that most of the dissociation and binding events are detected in our single molecule measurements. We separately considered the possibility that we were missing very slow binding and dissociation events in our single molecule measurements of LexA and Gal4 binding to nucleosomes. We typically detect fluorescence for about 200 s before photobleaching. Of all molecules that had high a FRET signal, we never detected long-lived low or high FRET states. This strongly indicates that there were little to no slow binding or dissociation events.

3.5. Data analysis

The image series acquired by the EMCCD camera was analyzed using ImageJ and custom written Matlab programs. The positions of individual fluorescent molecules in the image were identified by doing a 2-D peak search and filtering through appropriate threshold values. The single-molecule fluorescence emission intensity value for each molecule was calculated from the image by taking the average grey scale intensity value of a 3 pixel by 3 pixel region centered at the peak position identified from the previous step. The fluorescence emission time series of the Cy3 and Cy5 channels were then generated from the image series for each molecule (Fig. 4A). For the nucleosome FRET experiments, the single-molecule FRET efficiency was calculated using $E = I_A / (I_A + \gamma I_D)$, where I_D and I_A are the emission intensities from Cy3 and Cy5 at each time point, respectively, after background subtraction. γ is the detection correction factor and it can be determined by the ratio of the donor and acceptor emission intensity changes before (*pre*) and after (*post*) the acceptor photobleaching as: $\gamma = (I_A^{pre} - I_A^{post}) / (I_D^{post} - I_D^{pre})$ [55].

The intrinsic unwrapping fluctuations of the nucleosome happen at a much faster time scale than the exposure time used on the EMCCD camera, and thus cannot be captured. The FRET efficiency of the nucleosome stays at a high level around 0.8 in the absence of TF. After the addition of TF, the binding of TFs traps the nucleosome in the open state with a FRET efficiency of ~ 0.2 for a time scale long enough to be detected. The FRET time series shows fluctuations between the high and low FRET efficiency states upon the binding and dissociation of the TF (Fig. 4B). We

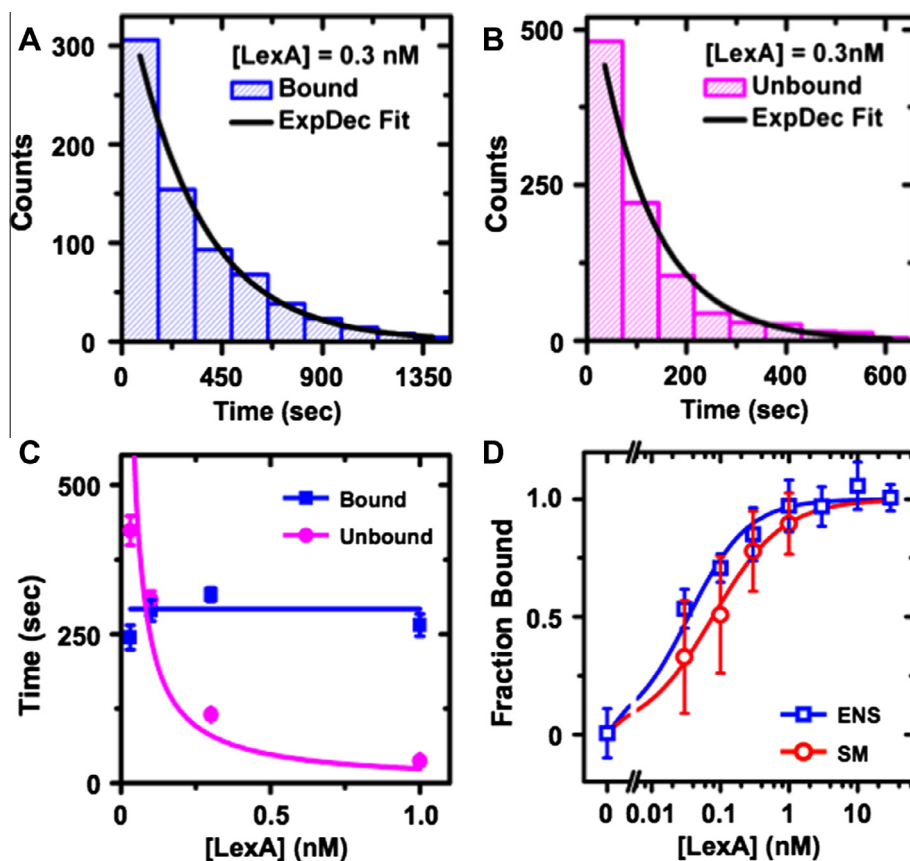


Fig. 5. Dwell time histograms of dsDNA with 0.3 nM LexA in the bound (A) and unbound (B) TF states, which were determined from single-molecule PIFE traces such as the ones shown in Fig. 4C. The distribution was fit with a single exponential decay (black line). (C) The bound (blue square) and unbound (magenta circle) LexA dwell times, t_{bound} and $t_{unbound}$, plotted as a function of LexA concentration. Each dwell time was determined by fitting the distribution histogram with a single exponential decay as shown in A and B. The bound state dwell times were fit as a constant and the unbound state dwell times were fit as $t = A/[LexA]$. (D) The fraction of dsDNA bound by LexA as determined from ensemble PIFE measurements (blue square) and single-molecule measurements (red circle). The data were fit with a noncooperative binding curve.

determined the location of each potential nucleosome molecule from the co-localization of fluorescence signal in the Cy3 and Cy5 images. Among these molecules we determined, which molecules exhibited the high FRET state. This allowed us to eliminate nucleosomes that were partially to fully disassembled. We found that about 70% of these nucleosomes with a high FRET efficiency state exhibited FRET efficiency fluctuations in the presence of TF. In order to obtain the binding and dissociation rate constants, the single-molecule FRET efficiency time series was fit to step functions by hidden Markov method (HMM), using the custom written Matlab program vbFRET [56] provided by Dr. Ruben Gonzalez (Columbia University). The number of FRET states was limited to two during the fitting, a high FRET state for the TF unbound state, and a low FRET state for the TF bound state, as observed in the raw FRET time series. The HMM fitting gives a final idealized FRET trace for each raw FRET time series (Fig. 4A).

The single-molecule PIFE data for TF binding to the naked DNA were analyzed similarly to the FRET data. In this case, only the Cy3 emission time series was used for HMM analysis. The Cy3 emission intensity was stable and stayed at the base level before photobleaching in the absence of TF. With the addition of TF, intensity fluctuation in Cy3 emission was observed (Fig. 4C). The Cy3 emission intensity is increased by approximately a factor of 2 or 1.5 when a LexA or Gal4 protein is bound, respectively. About 25% of the DNA molecules that have both Cy3 and Cy5 emission exhibit this PIFE fluctuation with LexA, and these molecules were included in the data analysis. The number of states was again limited to two during HMM fitting, where the high intensity state was the TF

bound state and low intensity state was the TF unbound state. During both nucleosome and DNA experiments, a fraction of the molecules identified by co-localization of Cy3 and Cy5 fluorophores did not show any fluctuation in FRET or PIFE in the presence of TF. This could be caused by non-specific interaction between the sample molecule and the microscope slide surface. These inactive molecules could be trapped on the slide surface such that they could not accommodate the binding of TF to the specific site. Only molecule that showed FRET or PIFE fluctuation were included in HMM analysis.

The TF bound and unbound dwell time distribution histogram was obtained from the idealized FRET or PIFE time series generated by HMM analysis. For the DNA experiment with LexA, the high emission state is the TF bound state (Fig. 5A) and the low emission state is the TF unbound state (Fig. 5B), whereas for the mono-nucleosome FRET experiments with LexA, the low FRET state is the TF bound state (Fig. 6A) and the high FRET state is the TF unbound state (Fig. 6B). The dwell time histogram was fit to single-exponential decay and the decay constant was the characteristic time constant of the TF bound state (τ_{bound}) or unbound state ($\tau_{unbound}$). Titration in LexA concentration was performed for both DNA and nucleosome experiments and the τ_{bound} and $\tau_{unbound}$ for LexA binding to DNA and nucleosome were obtained at these different LexA concentrations. The same type of single-molecule experiments were also repeated for LexA binding to di-nucleosome array, as well as Gal4 binding to mono-nucleosome [25]. τ_{bound} does not change with the TF concentration in DNA (Fig. 5C) or nucleosome (Fig. 6C) experiments. The concentration independent

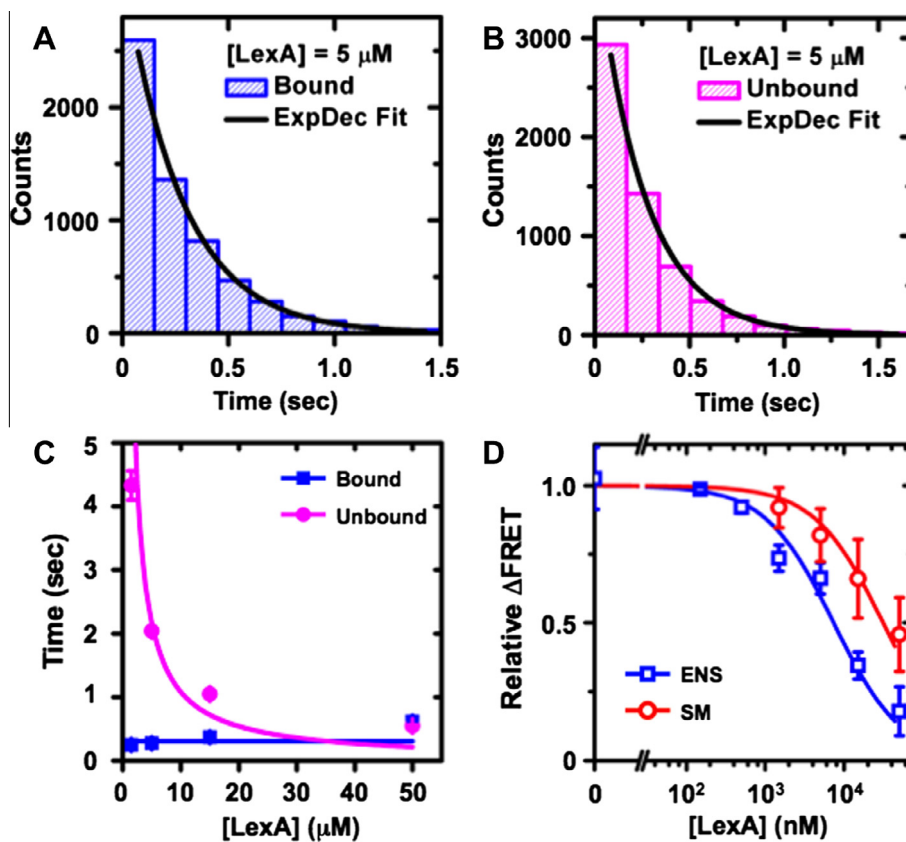


Fig. 6. Dwell time histogram of nucleosomes with 5 mM LexA in the bound (A) and unbound (B) TF states, which were determined from the single-molecule FRET traces such as the ones shown in Fig. 4B. The distribution was fit with a single exponential decay (black line). (C) The bound (blue square) and unbound (magenta circle) LexA dwell times, t_{bound} and $t_{unbound}$, plotted as a function of LexA concentration. Each dwell time was determined by fitting the distribution histogram with a single exponential decay as shown in A and B. The bound state dwell times were fit as a constant and the unbound state dwell times were fit as $t = A/[LexA]$. (D) The relative FRET efficiency of the nucleosome as determined from ensemble FRET measurements (blue square) and single-molecule measurements (red circle). Data were fit with a noncooperative binding curve (dose response curve).

τ_{bound} was fit to a constant. The inverse of this time constant gives the dissociation rate constant $k_{off} = 1/\tau_{bound}$. The TF concentration dependence of $\tau_{unbound}$ fits well to a hyperbolic curve $\tau_{unbound} = A/[TF]$ (Figs. 5C and 6C), where the inverse of constant A gives the binding rate constant $k_{on} = 1/A$. The dissociation constant K_D was then calculated from k_{on} and k_{off} as $K_D = k_{off}/k_{on}$. These kinetic parameters measured on the single-molecule level for the LexA and Gal4 binding to DNA, mono-nucleosome and di-nucleosome arrays are summarized in Table 2.

To confirm that these single molecule FRET measurements of TF binding and dissociation kinetics within nucleosomes were not significantly influenced by the surface attachment and that our ensemble of FRET fluctuations is representative of the events that occur in bulk measurements, we compared the $S_{0.5}$ determined by ensemble and single molecule measurements. The average TF occupancy was obtained from the single-molecule time series and then compared to the results from ensemble measurements. For FRET labeled nucleosomes, the fraction of nucleosomes unbound can be defined as $F_{unbound} = \sum_{\text{all molecules}} t_{high} / \sum_{\text{all molecules}} (t_{low} + t_{high})$, where t_{high} and t_{low} are the total lengths of time each molecule is in the high FRET (TF unbound) and low FRET (TF bound) states respectively. For TF binding to naked dsDNA detected by PIFE, the fraction of DNA molecules bound is $F_{bound} = \sum_{\text{all molecules}} t_{high} / \sum_{\text{all molecules}} (t_{low} + t_{high})$, where t_{high} is now the total length of time the molecule stays in the high Cy3 emission state (TF bound), and t_{low} is the total length of time the DNA molecule is in the low Cy3 emission state (TF unbound). This was repeated for each TF concentration in the titration, and then the data were fit to a noncooperative ligand-binding curve (Fig. 5D, Fig. 6D). The single-molecule nucleosome $F_{unbound}$ and DNA F_{bound} data were then compared to the data from ensemble measurements on a normalized scale. The TF binding curves determined from single-molecule fluorescence time series are similar to the ensemble results [25], with a $S_{0.5}$ that is within a factor of 2 for DNA and 4 for nucleosomes (Table 2). This scale of difference is typical for $S_{0.5}$ measurements by distinct methodologies. A potential reason that the single molecule measurements detect a higher $S_{0.5}$ is that the single molecule measurements are done in long narrow channels with a high surface to volume ratio, which could result in a higher loss of TF to nonspecific binding to the channel surfaces. The similarity between the single-molecule and ensemble $S_{0.5}$ measurements indicates that the surface tethering does not significantly impact the TF binding and dissociation dynamics and that the kinetic parameters obtained from immobilized nucleosomes can be used to assess TF binding dynamics of free nucleosome in solution.

4. Conclusion

Single molecule fluorescence measurements directly detect the binding and dissociation of DNA binding proteins to their target sites in equilibrium. Comparison of the binding and dissociation rates between a target site within naked DNA and a nucleosome allows for the determination of the influence of the nucleosome on both binding and dissociation. Here, we described smTIRF measurements of DNA binding TFs that determined nucleosomes significantly impact both TF binding and dissociation rates. These methodologies should be applicable to many protein complexes that bind DNA within chromatin and regulate DNA processing including DNA replication, repair and transcription.

Acknowledgments

The authors thank Ralf Bundschuh, Cai Chen, Jennifer Ottesen and members from the Poirier Lab for helpful discussions. We

are grateful for the advice from Rubin Gonzalez on setting up the smTIRF system, flow cell preparation and data analysis. The histone and LexA expression vectors were generous gifts from Jonathan Widom and Karolin Luger. This work was funded by the National Institutes of Health GM083055 (M.G.P.), American Heart Association Predoctoral Fellowship 0815460D and OSUCCC Pelotonia Fellowship (J.A.N.).

References

- [1] K. Luger, A.W. Mader, R.K. Richmond, D.F. Sargent, T.J. Richmond, *Nature* 389 (6648) (1997) 251–260.
- [2] K. Luger, M.L. Dechassa, D.J. Tremethick, *Nat. Rev. Mol. Cell Biol.* 13 (7) (2012) 436–447.
- [3] B. Li, M. Carey, J.L. Workman, *Cell* 128 (4) (2007) 707–719.
- [4] S.G. Swygert, C.L. Peterson, *Biochim. Biophys. Acta* (2014).
- [5] M.J. Guertin, J.T. Lis, *Curr. Opin. Genet. Dev.* 23 (2) (2013) 116–123.
- [6] N. Avvakumov, A. Nourani, J. Cote, *Mol. Cell* 41 (5) (2011) 502–514.
- [7] G.J. Narlikar, R. Sundaramoorthy, T. Owen-Hughes, *Cell* 154 (3) (2013) 490–503.
- [8] K.J. Polach, J. Widom, *J. Mol. Biol.* 254 (2) (1995) 130–149.
- [9] G. Li, J. Widom, *Nat. Struct. Mol. Biol.* 11 (8) (2004) 763–769.
- [10] C.L. White, K. Luger, *J. Mol. Biol.* 342 (5) (2004) 1391–1402.
- [11] Y.J. Park, P.N. Dyer, D.J. Tremethick, K. Luger, *J. Biol. Chem.* 279 (23) (2004) 24274–24282.
- [12] J.D. Anderson, J. Widom, *J. Mol. Biol.* 296 (4) (2000) 979–987.
- [13] G. Li, M. Levitus, C. Bustamante, J. Widom, *Nat. Struct. Mol. Biol.* 12 (1) (2005) 46–53.
- [14] H.S. Tims, K. Gurunathan, M. Levitus, J. Widom, *J. Mol. Biol.* 411 (2) (2011) 430–448.
- [15] H.S. Tims, J. Widom, *Methods* 41 (3) (2007) 296–303.
- [16] M. Tomschik, K. van Holde, J. Zlatanova, *J. Fluoresc.* 19 (1) (2009) 53–62.
- [17] J.Y. Lee, T.H. Lee, *J. Am. Chem. Soc.* 134 (1) (2012) 173–175.
- [18] W.J. Koopmans, A. Brehm, C. Logie, T. Schmidt, J. van Noort, *J. Fluoresc.* 17 (6) (2007) 785–795.
- [19] T.R. Blosser, J.G. Yang, M.D. Stone, G.J. Narlikar, X. Zhuang, *Nature* 462 (7276) (2009) 1022–1027.
- [20] M.L. Visnapuu, E.C. Greene, *Nat. Struct. Mol. Biol.* 16 (10) (2009) 1056–1062.
- [21] S. Deindl, W.L. Hwang, S.K. Hota, T.R. Blosser, P. Prasad, B. Bartholomew, X. Zhuang, *Cell* 152 (3) (2013) 442–452.
- [22] H. Neumann, S.M. Hancock, R. Buning, A. Routh, L. Chapman, J. Somers, T. Owen-Hughes, J. van Noort, D. Rhodes, J.W. Chin, *Mol. Cell* 36 (1) (2009) 153–163.
- [23] J.C. Shimko, J.A. North, A.N. Bruns, M.G. Poirier, J.J. Ottesen, *J. Mol. Biol.* 408 (2) (2011) 187–204.
- [24] J.A. North, J.C. Shimko, S. Javaid, A.M. Mooney, M.A. Shoffner, S.D. Rose, R. Bundschuh, R. Fishel, J.J. Ottesen, M.G. Poirier, *Nucleic Acids Res.* (2012).
- [25] Y. Luo, J.A. North, S.D. Rose, M.G. Poirier, *Nucleic Acids Res.* 42 (5) (2014) 3017–3027.
- [26] O. Ecevit, M.A. Khan, D.J. Goss, *Biochemistry* 49 (12) (2010) 2627–2635.
- [27] Y. Liu, A. Schepartz, *Biochemistry* 40 (21) (2001) 6257–6266.
- [28] K.M. Parkhurst, M. Brenowitz, L.J. Parkhurst, *Biochemistry* 35 (23) (1996) 7459–7465.
- [29] A. Thastrom, J.M. Gottesfeld, K. Luger, J. Widom, *Biochemistry* 43 (3) (2004) 736–741.
- [30] D. Skoko, B. Wong, R.C. Johnson, J.F. Marko, *Biochemistry* 43 (43) (2004) 13867–13874.
- [31] J.S. Graham, R.C. Johnson, J.F. Marko, *Nucleic Acids Res.* 39 (6) (2011) 2249–2259.
- [32] C.E. Sing, M. Olvera de la Cruz, J.F. Marko, *Nucleic Acids Res.* (2014).
- [33] M.J. McCauley, E.M. Rueter, I. Rouzina, L.J. Maher 3rd, M.C. Williams, *Nucleic Acids Res.* 41 (1) (2013) 167–181.
- [34] R. Gamsjaeger, M.R. O'Connell, L. Cubeddu, N.E. Shepherd, J.A. Lowry, A.H. Kwan, M. Vandevenne, M.K. Swanton, J.M. Matthews, J.P. Mackay, *J. Biol. Chem.* 288 (49) (2013) 35180–35191.
- [35] M. Munde, G.M. Poon, W.D. Wilson, *J. Mol. Biol.* 425 (10) (2013) 1655–1669.
- [36] B. Dey, S. Thukral, S. Krishnan, M. Chakrobarty, S. Gupta, C. Manghani, V. Rani, *Mol. Cell. Biochem.* 365 (1–2) (2012) 279–299.
- [37] A.M. van Oijen, *Curr. Opin. Biotechnol.* 22 (1) (2011) 75–80.
- [38] Y.S. Lin, M.F. Carey, M. Ptashne, M.R. Green, *Cell* 54 (5) (1988) 659–664.
- [39] I. Albert, T.N. Mavrich, L.P. Tomsho, J. Qi, S.J. Zanton, S.C. Schuster, B.F. Pugh, *Nature* 446 (7135) (2007) 572–576.
- [40] K.D. MacIsaac, T. Wang, D.B. Gordon, D.K. Gifford, G.D. Stormo, E. Fraenkel, *BMC Bioinformatics* 7 (2006) 113.
- [41] C. Jiang, B.F. Pugh, *Genome Biol.* 10 (10) (2009) R109.
- [42] R.M. Clegg, *Methods Enzymol.* 211 (1992) 353–388.
- [43] A.J. Andrews, X. Chen, A. Zevin, L.A. Stargell, K. Luger, *Mol. Cell* 37 (6) (2010) 834–842.
- [44] A. Flaus, K. Luger, S. Tan, T.J. Richmond, *Proc. Natl. Acad. Sci. U.S.A.* 93 (4) (1996) 1370–1375.
- [45] B. Dorigo, T. Schalch, A. Kulangara, S. Duda, R.R. Schroeder, T.J. Richmond, *Science* 306 (5701) (2004) 1571–1573.
- [46] P.J. Robinson, L. Fairall, V.A. Huynh, D. Rhodes, *Proc. Natl. Acad. Sci. U.S.A.* 103 (17) (2006) 6506–6511.

- [47] R.A. Rogge, A.A. Kalashnikova, U.M. Muthurajan, M.E. Porter-Goff, K. Luger, J.C. Hansen, *J. Vis. Exp.* 79 (2013).
- [48] M.G. Poirier, E. Oh, H.S. Tims, J. Widom, *Nat. Struct. Mol. Biol.* 16 (9) (2009) 938–944.
- [49] R. Roy, S. Hohng, T. Ha, *Nat. Methods* 5 (6) (2008) 507–516.
- [50] H. Hwang, H. Kim, S. Myong, *Proc. Natl. Acad. Sci. U.S.A.* 108 (18) (2011) 7414–7418.
- [51] K. Luger, T.J. Rechsteiner, T.J. Richmond, *Methods Enzymol.* 304 (1999) 3–19.
- [52] J.W. Little, B. Kim, K.L. Roland, M.H. Smith, L.L. Lin, S.N. Slilaty, *Methods Enzymol.* 244 (1994) 266–284.
- [53] R. Dave, D.S. Terry, J.B. Munro, S.C. Blanchard, *Biophys. J.* 96 (6) (2009) 2371–2381.
- [54] M. Bates, T.R. Blosser, X. Zhuang, *Phys. Rev. Lett.* 94 (10) (2005) 108101.
- [55] J.J. McCann, U.B. Choi, L. Zheng, K. Weninger, M.E. Bowen, *Biophys. J.* 99 (3) (2010) 961–970.
- [56] J.E. Bronson, J. Fei, J.M. Hofman, R.L. Gonzalez Jr., C.H. Wiggins, *Biophys. J.* 97 (12) (2009) 3196–3205.